Fermi-level stabilization in the topological insulators Bi_2Se_3 and Bi_2Te_3: Origin of the surface electron gas

Joonki Suh,[1] Deyi Fu,[1] Xinyu Liu,[2] Jacek K. Furdyna,[2] Kin Man Yu,[3] Wladyslaw Walukiewicz,[3] and Junqiao Wu[1,3]
[1]*Department of Materials Science and Engineering, University of California, Berkeley, California 94720, USA*
[2]*Department of Physics, University of Notre Dame, Notre Dame, Indiana 46556, USA*
[3]*Materials Sciences Division, Lawrence Berkeley National Laboratory, Berkeley, California 94720, USA*
(Received 13 December 2013; revised manuscript received 30 January 2014; published 10 March 2014)

Two-dimensional electron gas (2DEG) coexists with topological states on the surface of topological insulators (TIs), while the origin of the 2DEG remains elusive. In this work, electron density in TI thin films (Bi_2Se_3, Bi_2Te_3, and their alloys) were manipulated by controlling the density of electronically active native defects with particle irradiation. The measured electron concentration increases with irradiation dose but saturates at different levels for Bi_2Se_3 and Bi_2Te_3. The results are in quantitative agreement with the amphoteric defect model, which predicts that electronically active native defects shift the Fermi energy (E_F) toward a Fermi stabilization level (E_{FS}) located universally at ~4.9 eV below the vacuum level. Combined with thickness-dependent data, it is demonstrated that regardless of the bulk doping, the surface E_F is always pinned at E_{FS}, producing a band bending and 2DEG on TI film surfaces. Our work elucidates native defect physics of TIs with a model universally applicable to other semiconductors and has critical implications for potential device applications of TIs.

DOI: 10.1103/PhysRevB.89.115307 PACS number(s): 73.20.−r, 61.82.Fk, 73.25.+i

I. INTRODUCTION

Topological insulators (TIs) are of great interest owing to the topologically protected gapless surface states [1,2]. The novel topological surface states have been extensively studied, and their existence has been experimentally confirmed by angle-resolved photoemission spectroscopy (ARPES) [3,4], scanning tunneling microscopy (STM) [5,6], and corresponding transport measurements [7,8]. Furthermore, they have the possibility of hosting novel physical phenomena, including Majorana fermions [9], magnetic monopoles [10], and quantum anomalous Hall effect [11], as well as promising applications in spintronics and quantum computing. Bi_2Se_3 and Bi_2Te_3 are representative examples of such three-dimensional TIs, and their ternary alloys $Bi_2(Se_{1-x}Te_x)_3$ have also been demonstrated to display TI properties [12].

More recently, the coexistence of two distinctive types of surface conducting channels has been observed in both Bi_2Se_3 [13,14] and Bi_2Te_3 [15,16], with one being Dirac electrons from the topological state and the other from a two-dimensional electron gas (2DEG). The latter has been often attributed to a conventional band-bending effect, without specifying its physical origin. As another possible explanation, an epitaxial bismuth bilayer (Bi_2) on top of bulk TIs has been hypothesized [17] and experimentally revealed by STM imaging [18]. However, the Bi bilayer formation was spatially nonuniform and triggered only by thermal activation; thus, it cannot support the spontaneous formation of 2DEG universally observed in this family of TIs.

In this paper, we present the first experimental evidence that the 2DEG in TIs is directly related to unavoidable native defects and associated dangling bonds present on the surface. The defect-induced pinning of surface Fermi energy was revealed through a combination of irradiation experiments, where we intentionally generate native defects in the bulk, and theoretical analysis, in terms of a widely applied defect model. In exploiting the unique properties of Tis, it is often necessary to interface them with other materials. Thus, this demonstration of native-defect-induced 2DEG on TIs is a significant step toward better understanding of the topological states and has important implications for applications of TIs in practical devices.

II. EXPERIMENTAL DETAILS

Thin films of Bi_2Se_3, Bi_2Te_3 and their ternary alloys were grown on semi-insulating GaAs (001) substrates with molecular beam epitaxy [19]. The composition of ternary compounds was controlled by varying Se_2 and Te_2 beam fluxes to cover the entire composition range. After growth, the thickness and composition of TI films were precisely determined by Rutherford backscattering spectrometry, while the crystal structure was characterized by high resolution x-ray diffraction (XRD) and ion channeling. X-ray diffraction measurements reveal the high crystal quality of these TI films with preferred crystal orientation along the c axis [Fig. 1(a)]. The existence of topological surface states in these films was confirmed by ARPES measurements [20].

Native point defects in the TI films were generated by irradiating the samples with energetic ions. In order to compare the degree of irradiation damage (and hence the density of generated native defects) by different species of ions, the displacement damage dose (D_d) approach was utilized by extracting nonionizing energy loss (NIEL) from Monte Carlo simulation with the Stopping Range of Ions in Matter (SRIM) program [21]. TI films were sequentially irradiated for D_d up to 2×10^{14} MeV/g with 3 MeV He^{2+} (up to an ion dose of 2×10^{15} cm^{-2}) and then for D_d, ranging from 1×10^{15} to 1×10^{17} MeV/g with 150 keV Ne^+ ions (with ion dose from $\sim 10^{13}$ to 10^{15} cm^{-2}). Also, the maximum thickness of TI films used for this irradiation study was restricted by the projected range (~180 nm in $Bi_2(Se_{1-x}Te_x)_3$) for the 150 keV Ne^+ irradiation. The thickness of the films in the irradiation study ranges from 29 to 116 nm. Thus, most of the He^{2+} and Ne^+ ions completely pass through the entire film thickness, leaving

 ©2014 American Physical Society

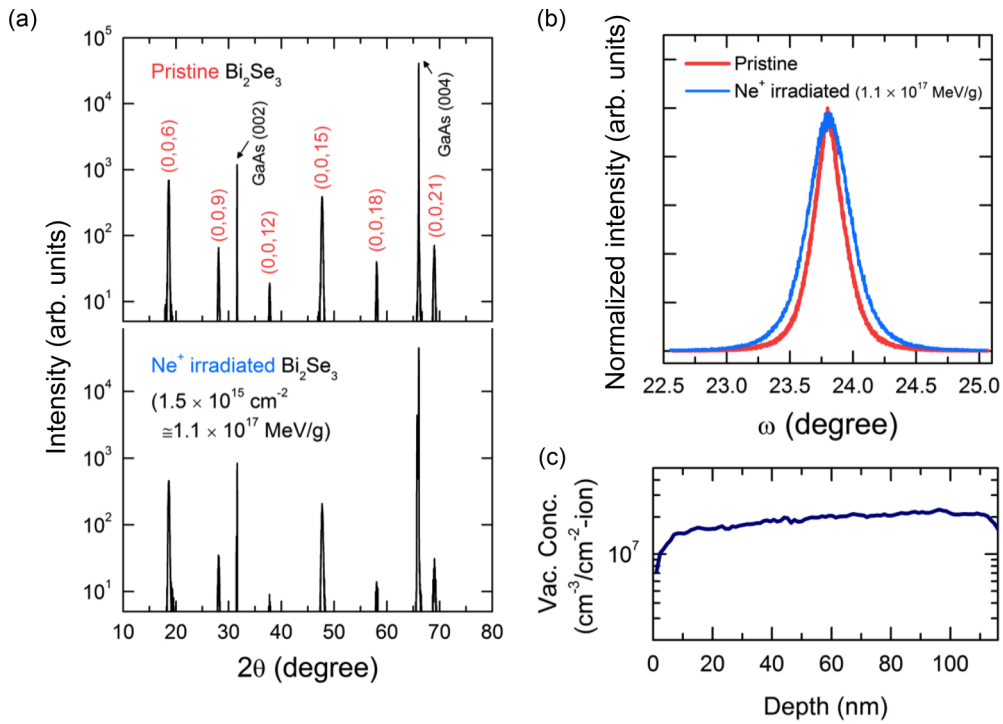

FIG. 1. (Color online) XRD spectra of a representative TI film. (a) θ-2θ scans. (b) Normalized ω rocking curves at (0,0,15) reflection of pristine film and Ne^+ irradiated at the highest displacement damage dose (D_d), 1.1×10^{17} MeV/g, of a 105-nm-thick Bi_2Se_3 film grown on semi-insulating GaAs (001) substrate. (c) SRIM-simulated depth profile of vacancy concentration generated by 150 keV Ne^+ bombardment in 116 nm Bi_2Te_3 film, the thickest film used in the irradiation experiment.

behind uniform damage throughout the film in both depth and lateral directions. SRIM predicts that the distribution of defect concentration is relatively uniform along the depth of TI films, even in the thickest 116-nm Bi_2Te_3 sample [Fig. 1(c)]. It was also confirmed that electrically, the semi-insulating GaAs substrate still remains highly insulating after the irradiation, so we can confine our discussion to irradiation-induced native defects in the TI films. The XRD pattern in Fig. 1(a) confirms that the high crystal quality of the film is still retained even after irradiation with the highest $D_d = 1.1 \times 10^{17}$ MeV/g, corresponding to Ne^+ irradiation with a high dose of 1.5×10^{15} cm^{-2}. All diffraction peaks indeed remain sharp, although the full-width at half-maximum of the rocking curve is slightly increased from 0.27 to 0.39°, as seen in Fig. 1(b). This is a clear indication that irradiation within the doses used in our work generates only native point defects (vacancies and interstitials) in the TI films and does not cause amorphization or formation of substantial amounts of extended defects.

III. RESULTS AND DISCUSSIONS

Figure 2 shows the evolution of electrical transport properties of Bi_2Se_3 and Bi_2Te_3, as native defects are introduced by irradiation, determined by room-temperature Hall effect measurements with a 0.6 T magnetic field in the van der Pauw configuration. The concentration of free electrons (n) in both binary TIs increases with increasing D_d, as shown in Fig. 2(a); the irradiation-induced native defects behave as donors in these narrow band-gap semiconductors. Accordingly, electron mobility is generally reduced due to increasing scattering events from the ionized native defects acting as charged scattering centers [Fig. 2(c)]. Assuming that surfaces already are already saturated with a high density of native defects associated with dangling bonds, the decrease of measured mobility is mainly caused by a decrease in the bulk mobility upon irradiation. We note that our measured room-temperature mobilities in pristine films are consistent with report values in literature [22,23]. With a further increase in damage dose, however, n ultimately saturates at a characteristic concentration (n_{sat}) that differs by more than an order of magnitude between Bi_2Se_3 ($n_{sat} \sim 3 \times 10^{19}$ cm^{-3}) and Bi_2Te_3 ($n_{sat} \sim 4 \times 10^{20}$ cm^{-3}). Regardless of film thicknesses that lead to different pristine n, the electron concentration is observed to saturate approximately at the same level [Fig. 2(b)]. This means that n_{sat} is an intrinsic property of the material, corresponding to a Fermi-level (E_F) stabilized at a specific energy position. We also note that D_d required to achieve the carrier saturation is proportional to film thickness due to greater bulk contribution in thicker films.

These observations can be well understood within the amphoteric defect model (ADM) developed based on E_F-dependent formation energy of native defects [24]. ADM predicts that the formation energy and the type (donor or acceptor) of dominant native defects in a semiconductor is controlled by the location of E_F relative to a nearly universal energy level located at about 4.9 eV below the vacuum level, termed the Fermi stabilization level (E_{FS}). Thus, donorlike (or acceptorlike) native defects are predominantly formed when $E_F < E_{FS}$ ($E_F > E_{FS}$). Consequently, for sufficiently high defect concentration, E_F stabilizes at E_{FS}, where the formation energies and incorporation rates of donorlike defects become equal to those of acceptorlike. The ADM concept with the universal E_{FS} has been successfully applied to a wide range of

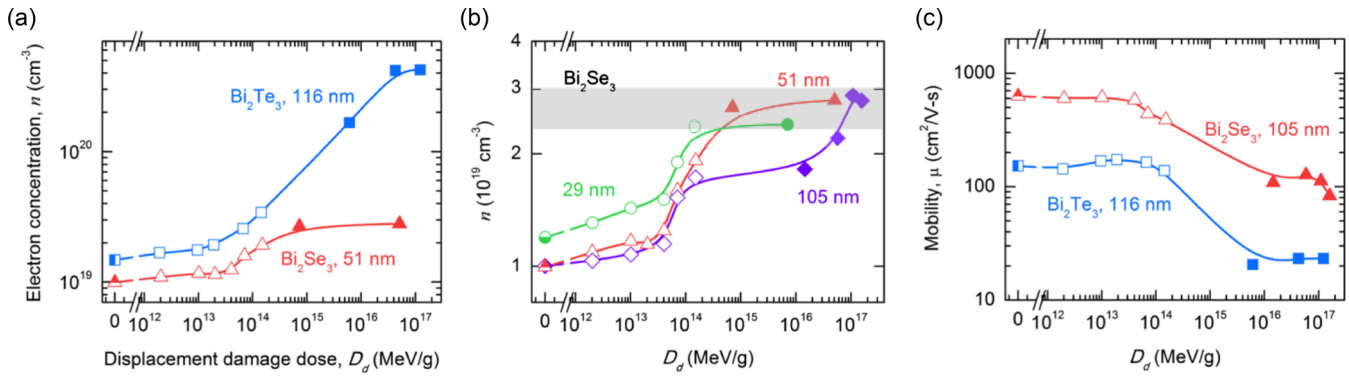

FIG. 2. (Color online) (a) Electron concentration, determined by Hall effect at room temperature, as a function of D_d in a Bi_2Se_3 (51 nm) and Bi_2Te_3 (116 nm) film. D_d was obtained by multiplying irradiation dose with NIEL calculated with SRIM. (b) Room-temperature electron concentration upon irradiation in three Bi_2Se_3 thin films with different thicknesses. The shaded region shows the approximate level where n saturates. (c) Carrier mobility as a function of D_d in a Bi_2Se_3 and Bi_2Te_3 film. All half-filled symbols correspond to pristine values. Open and filled symbols represent values measured on He^{2+} and Ne^{+} irradiated films, respectively. Solid lines are guides for the eye.

elemental and compound semiconductors [25]. Therefore, the location of E_F relative to the known E_{FS} is a key parameter to gauge electronic properties of native defects. First, the energies of band edges in Bi_2Te_3 can be deduced from its intrinsic band gap ($E_G{}^0 = 0.17$ eV) [26] and the work function (ϕ) of 5.3 eV measured in p-type Bi_2Te_3 when E_F is located at its valence-band maximum (VBM) [27]. As visualized in Fig. 3(a), $E_{FS} \sim 4.9$ eV is then situated deep inside the conduction band of Bi_2Te_3. Therefore, in our moderate n-type Bi_2Te_3 samples, $E_F < E_{FS}$ and donorlike native defects are predominantly generated during irradiation, shifting E_F up toward E_{FS}. Eventually, as shown in Fig. 2, the electron concentration saturates at n_{sat} when E_F reaches E_{FS}. Similar effects have been observed in other compound semiconductors with large electron affinity (χ), such as InN [28,29] and CdO [30,31]. On the other hand, to the best of our knowledge, the electron affinity of Bi_2Se_3 has not been experimentally determined yet. However, following the argument of ADM, we can use our results on the irradiation induced saturation of electron concentration to determine its electron affinity.

A quantitative determination of the band offset can be made using the ADM under the condition that $E_F = E_{FS}$ when $n = n_{sat}$. The relationship between n and E_F is given by [32],

$$n = \frac{2}{8\pi^3}\iiint \frac{1}{1+\exp[(E_C - E_F)/k_B T]} d^3k, \quad (1)$$

where the electron energy E_C is related to wave vector k via the nonparabolic dispersion by solving Kane's two-band model [33],

$$E_C(k) = E_G + \frac{\hbar^2 k^2}{2m_0} + \frac{1}{2}\left(\sqrt{E_G^2 + 4E_P \cdot \frac{\hbar^2 k^2}{2m_0}} - E_G\right). \quad (2)$$

Here, E_P is an energy parameter related to the interaction momentum matrix element and approximately determined through the $k \cdot p$ result,

$$\frac{m_e^*}{m_0} \approx \frac{E_G}{E_P}. \quad (3)$$

We have also taken into account the conduction-band renormalization effects at high n due to electron-electron interaction (ΔE_{e-e}) and electron-ionized impurity interaction (ΔE_{e-i}), given by the following expression [34]:

$$\Delta E_{e-e} = -\frac{2e^2 k_F}{\pi \varepsilon_S} - \frac{e^2 k_{TF}}{2\varepsilon_S}\left[1 - \frac{4}{\pi}\arctan\left(\frac{k_F}{k_{TF}}\right)\right], \quad (4)$$

$$\Delta E_{e-i} = -\frac{4\pi e^2 n}{\varepsilon_S a_B k_{TF}^3}, \quad (5)$$

where $k_F = (3\pi^2 n)^{1/3}$ is the Fermi wave vector, $k_{TF} = (2/\sqrt{\pi})(k_F/a_B)^{1/2}$ is the Thomas-Fermi screening wave vector, ε_S is the static dielectric constant, and a_B is the Bohr radius (angstrom). We note that even at $n = n_{sat} \sim 4 \times 10^{20}$ cm^{-3}, the renormalization-caused downshift of conduction-band minimum (CBM) is equal to only ~0.024 eV (hence, E_G narrows to 0.146 eV) in Bi_2Te_3; this is due to the large ε_S of 290 [35] and to the multiplicity of the effective conduction-band valleys ($N = 12$) that include the secondary conduction-band edges located very close to CBM [36]. With our measured n and literature value of $m_e^*/m_0 \sim 0.07$ in Bi_2Te_3 [36], E_F relative to CBM is calculated as a function of D_d [Fig. 3(b)]. The results are in quantitative agreement with ADM in that E_F stabilizes exactly at $E_{FS} = 4.9$ eV at high irradiation doses. Using the universality of E_{FS} among different materials, the same quantitative treatment is applied to Bi_2Se_3, with parameter values found in literature ($\varepsilon_S = 13, N = 1$, and $m_e^*/m_0 \sim 0.13$) [35,37,38], and the results are presented in Fig. 3. With this ADM approach, χ of Bi_2Se_3 is found to be ~5.06 eV, giving a VBM of ~0.08 eV lower than that of Bi_2Te_3, thus forming a type-I band offset between Bi_2Se_3 and Bi_2Te_3. This ADM-enabled quantitative treatment for Bi_2Se_3 (Bi_2Te_3) is in good agreement with the reported downward band bending of 0.13 eV (0.23 eV) caused by 2DEG when E_F in the bulk is located close to the CBM [15,39].

The successful application of ADM has an important implication for understanding the origin of 2DEG on the TI surfaces. ADM predicts that E_F on natural surfaces of semiconductors is pinned at E_{FS} due to abundant surface defects and dangling bonds with similar origin and properties as the native bulk

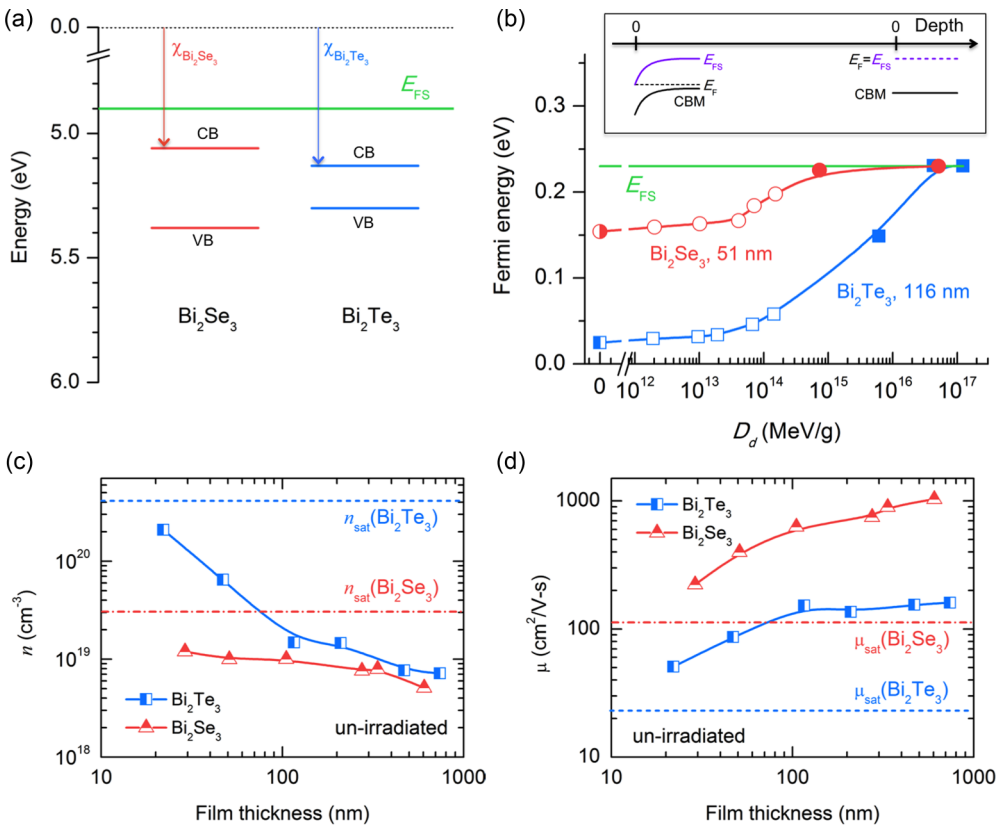

FIG. 3. (Color online) (a) Schematic representation of the Fermi stabilization position (E_{FS}), conduction-band edge (CBM), and valence-band edge (VBM) in Bi_2Se_3 and Bi_2Te_3. (b) Bulk Fermi level, measured from the CBM of Bi_2Te_3, moving toward E_{FS} as a function of D_d in Bi_2Se_3 and Bi_2Te_3. Inset shows schematics of band diagram along the depth of the samples, in the pristine (left) and Fermi-level-stabilized (right) TI films. All half-filled symbols correspond to the pristine values. Open and filled symbols represent values measured on He^{2+} and Ne^{+} irradiated films, respectively. (c) Electron concentration and (d) carrier mobility of pristine (unirradiated) TI films as a function of thickness. The saturated carrier densities and mobilities of Bi_2Te_3 and Bi_2Se_3 are obtained from Fig. 2.

defects. This prediction has been confirmed by the observed dependence of Schottky barrier height on semiconductor band-edge locations [40], as well as the formation of 2DEG in the accumulation layer in semiconductors having a CBM below E_{FS} (e.g., InN [41] and CdO [30]). In both cases, there was good agreement between the location of E_F on the surface and E_F in the bulk of heavily irradiated materials, potentially correlating the irradiation results to previously reported 2DEG formation by metal deposition [42].

To confirm the correlation between bulk and surface Fermi level stabilization energy, we have measured the thickness dependence of the electron concentration and mobility measured in as-grown Bi_2Te_3 and Bi_2Se_3 films. As shown in Figs. 3(c) and 3(d), the electron concentrations increase with decreasing thickness and tend toward n_{sat} in the low thickness limit in both materials. In contrast, the mobilities decrease with a decreasing sample thickness, but again they converge on the mobility values measured in thick, heavily irradiated materials. The electrical properties of thick samples are determined by the bulk with negligible contribution from the surface-interface layers. The bulk contribution decreases with decreasing film thickness, and in the limit of very thin samples, their electrical properties are determined by charge transport in the surface-interface layers. The observed clear tendency for both electron concentration and mobility to converge on the values of heavily irradiated thick samples confirms that E_F on the surface-interface of the studied TIs is pinned at E_{FS}, leading to accumulation of electrons and formation of the 2DEG.

To further show the difference between Bi_2Se_3 and Bi_2Te_3, the ternary alloy system $Bi_2(Se_{1-x}Te_x)_3$ in the full composition range ($0 \le x \le 1$) was also investigated with He^{2+} and Ne^{+} irradiation. As shown in Fig. 4(a), all these alloys exhibit

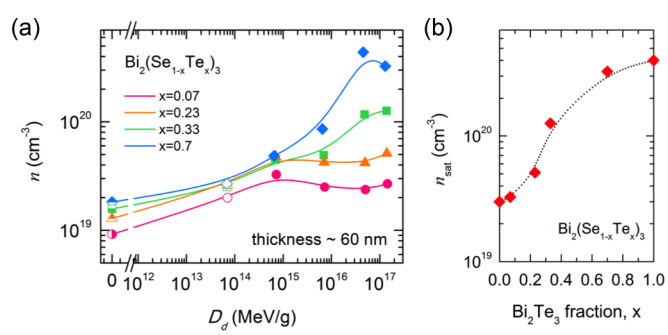

FIG. 4. (Color online) (a) Electron concentration as a function of D_d in a series of $Bi_2(Se_{1-x}Te_x)_3$ alloys with equal thickness of 60 nm. (b) Observed saturated electron concentration of $Bi_2(Se_{1-x}Te_x)_3$ as a function of x, the Bi_2Te_3 fraction.

the stabilization of n at sufficiently high irradiation doses corresponding to the condition of $E_F = E_{FS}$. Figure 4(b) illustrates the characteristic n_{sat} of these $Bi_2(Se_{1-x}Te_x)_3$ alloys with constant film thickness of ~60 nm. n_{sat} is strongly dependent on the composition x, increasing monotonically from 3×10^{19} in Bi_2Se_3 to 4×10^{20} cm^{-3} in Bi_2Te_3.

IV. SUMMARY

In conclusion, high-energy particle irradiation was used to show that intentionally introduced native defects tend to stabilize the Fermi level in the conduction band in TIs Bi_2Se_3, Bi_2Te_3 and their alloys. The measured electron density and mobility saturate with the Femi level stabilization at high doses of irradiation and is a trend that is also observed with decreasing thickness in pristine films. This indicates that the defects and dangling bonds abundant on the surface and/or interfaces will result in formation of electron accumulation layers and 2DEG. The finding explains difficulties in previous attempts to decouple electrical properties of TIs and has important implications for potential applications that utilize the unique dispersion relation of the topological states on the surface of these materials.

ACKNOWLEDGMENTS

This work was supported by the Office of Science, Office of Basic Energy Sciences of the US Department of Energy under Contract No. DE-AC02-05CH11231. The work at Notre Dame was supported by the National Science Foundation (Grant No. DMR10-05851). We thank J. Beeman and D. Detert for film irradiation and helpful discussions.

[1] L. Fu, C. L. Kane, and E. J. Mele, Phys. Rev. Lett. **98**, 106803 (2007).
[2] J. Moore, Nat. Phys. **5**, 378 (2009).
[3] D. Hsieh, Y. Xia, D. Qian, L. Wray, J. H. Dil, F. Meier, J. Osterwalder, L. Patthey, J. G. Checkelsky, N. P. Ong, A. V. Fedorov, H. Lin, A. Bansil, D. Grauer, Y. S. Hor, R. J. Cava, and M. Z. Hasan, Nature (London) **460**, 1101 (2009).
[4] Y. L. Chen, J. G. Analytis, J.-H. Chu, Z. K. Liu, S.-K. Mo, X. L. Qi, H. J. Zhang, D. H. Lu, X. Dai, Z. Fang, S. C. Zhang, I. R. Fisher, Z. Hussain, and Z.-X. Shen, Science **325**, 178 (2009).
[5] T. Zhang, P. Cheng, X. Chen, J.-F. Jia, X. Ma, K. He, L. Wang, H. Zhang, X. Dai, Z. Fang, X. Xie, and Q.-K. Xue, Phys. Rev. Lett. **103**, 266803 (2009).
[6] Z. Alpichshev, J. G. Analytis, J.-H. Chu, I. R. Fisher, Y. L. Chen, Z. X. Shen, A. Fang, and A. Kapitulnik, Phys. Rev. Lett. **104**, 016401 (2010).
[7] D. Kim, S. Cho, N. P. Butch, P. Syers, K. Kirshenbaum, S. Adam, J. Paglione, and M. S. Fuhrer, Nature Phys. **8**, 459 (2012).
[8] N. Bansal, Y. S. Kim, M. Brahlek, E. Edrey, and S. Oh, Phys. Rev. Lett. **109**, 116804 (2012).
[9] L. Fu and C. L. Kane, Phys. Rev. Lett. **100**, 096407 (2008).
[10] X.-L. Qi, R. Li, J. Zang, and S.-C. Zhang, Science **323**, 1184 (2009).
[11] R. Yu, W. Zhang, H.-J. Zhang, S.-C. Zhang, X. Dai, and Z. Fang, Science **329**, 61 (2010).
[12] J. J. Cha, D. Kong, S.-S. Hong, J. G. Analytis, K. Lai, and Y. Cui, Nano Lett. **12**, 1107 (2012).
[13] M. Bianchi, D. Guan, S. Bao, J. Mi, B. B. Iversen, P. D. C. King, and P. Hofmann, Nat. Commun. **1**, 128 (2010).
[14] C. E. ViolBarbosa, C. Shekhar, B. Yan, S. Ouardi, E. Ikenaga, G. H. Fecher, and C. Felser, Phys. Rev. B **88**, 195128 (2013).
[15] C. Chen, S. He, H. Weng, W. Zhang, L. Zhao, H. Liu, X. Jia, D. Mou, S. Liu, J. He, Y. Peng, Y. Feng, Z. Xie, G. Liu, X. Dong, J. Zhang, X. Wang, Q. Peng, Z. Wang, S. Zhang *et al.*, Proc. Natl. Acad. Sci. USA **109**, 3694 (2012).
[16] M. T. Pettes, J. Maassen, I. Jo, M. S. Lundstrom, and L. Shi, Nano Lett. **13**, 5316 (2013).
[17] X. He, W. Zhou, Z. Y. Wang, Y. N. Zhang, J. Shi, R. Q. Wu, and J. A. Yarmoff, Phys. Rev. Lett. **110**, 156101 (2013).
[18] P. M. Coelho, G. A. S. Ribeiro, A. Malachias, V. L. Pimentel, W. S. Silva, D. D. Reis, M. S. C. Mazzoni, and R. Magalhães-Paniago, Nano Lett. **13**, 4517 (2013).
[19] X. Y. Liu, D. J. Smith, H. L. Cao, Y. P. Chen, J. Fan, Y.-H. Zhang, R. E. Pimpinella, M. Dobrowolska, and J. K. Furdyna, J. Vac. Sci. Technol. B **30**, 02B103 (2012).
[20] X. Liu, Y. P. Chen, D. J. Smith, Y.-H. Zhang, C. Liu, M. Z. Hasan, M. Dobrowolska, J. K. Furdyna, J. Fan, H. Cao *et al.*, in *Bismuth-Containing Compounds* (Springer, New York, 2013), Vol. 186, p. 263.
[21] S. R. Messenger, E. A. Burke, G. P. Summers, M. A. Xapsos, R. J. Walters, E. M. Jackson, and B. D. Weaver, IEEE Trans. Nucl. Sci. **46**, 1595 (1999).
[22] N. P. Butch, K. Kirshenbaum, P. Syers, A. B. Sushkov, G. S. Jenkins, H. D. Drew, and J. Paglione, Phys. Rev. B **81**, 241301(R) (2010).
[23] H. Scherrer and S. Scherrer, in *Thermoelectrics Handbook: Macro to Nano*, edited by D. M. Rowe (CRC, Boca Raton, 2006), p. 27-1.
[24] W. Walukiewicz, Appl. Phys. Lett. **54**, 2094 (1989).
[25] W. Walukiewicz, Physica B **302**, 123 (2001).
[26] E. Kioupakis, M. L. Tiago, and S. G. Louie, Phys. Rev. B **82**, 245203 (2010).
[27] D. Haneman, J. Phys. Chem. Solids **11**, 205 (1959).
[28] S. X. Li, K. M. Yu, J. Wu, R. E. Jones, W. Walukiewicz, J. W. Ager, III, W. Shan, E. E. Haller, H. Lu, and W. J. Schaff, Phys. Rev. B **71**, 161201(R) (2005).
[29] A. X. Levander, T. Tong, K. M. Yu, J. Suh, D. Fu, R. Zhang, H. Lu, W. J. Schaff, O. Dubon, W. Walukiewicz, D. G. Cahill, and J. Wu, Appl. Phys. Lett. **98**, 012108 (2011).
[30] D. T. Speaks, M. A. Mayer, K. M. Yu, S. S. Mao, E. E. Haller, and W. Walukiewicz, J. Appl. Phys. **107**, 113706 (2010).
[31] P. D. C. King, T. D. Veal, P. H. Jefferson, J. Zúñiga-Pérez, V. Muñoz-Sanjosé, and C. F. McConville, Phys. Rev. B **79**, 035203 (2009).
[32] W. Zawadzki and W. Szymańska, Phys. Status Solidi B **45**, 415 (1971).
[33] E. O. Kane, J. Phys. Chem. Solids **1**, 249 (1957).
[34] J. Wu, W. Walukiewicz, W. Shan, K. M. Yu, J. W. Ager, III, E. E. Haller, H. Lu, and W. J. Schaff, Phys. Rev. B **66**, 201403 (2002).

[35] W. Richter, H. Kohler, and C. R. Becker, Phys. Status Solidi B **84**, 619 (1977).
[36] B.-L. Huang and M. Kaviany, Phys. Rev. B **77**, 125209 (2008).
[37] S. K. Mishra, S. Satpathy, and O. Jepsen, J. Phys.: Condens. Matter **9**, 461 (1997).
[38] J. G. Analytis, J.-H. Chu, Y. Chen, F. Corredor, R. D. McDonald, Z. X. Shen, and I. R. Fisher, Phys. Rev. B **81**, 205407 (2010).
[39] A. A. Taskin, S. Sasaki, K. Segawa, and Y. Ando, Phys. Rev. Lett. **109**, 066803 (2012).
[40] W. Walukiewicz, J. Vac. Sci. Technol. B **5**, 1062 (1987).
[41] J. Wu, W. Walukiewicz, S. X. Li, R. Armitage, J. C. Ho, E. R. Weber, E. E. Haller, H. Lu, W. J. Schaff, A. Barcz, and R. Jakiela, Appl. Phys. Lett. **84**, 2805 (2004).
[42] P. D. C. King, R. C. Hatch, M. Bianchi, R. Ovsyannikov, C. Lupulescu, G. Landolt, B. Slomski, J. H. Dil, D. Guan, J. L. Mi, E. D. L. Rienks, J. Fink, A. Lindblad, S. Svensson, S. Bao, G. Balakrishnan, B. B. Iversen, J. Osterwalder, W. Eberhardt, F. Baumberger *et al.*, Phys. Rev. Lett. **107**, 096802 (2011).